

# Modeling the dynamics of tidally-interacting binary neutron stars up to merger

Sebastiano Bernuzzi<sup>1,2</sup>, Alessandro Nagar<sup>3</sup>, Tim Dietrich<sup>4</sup>, and Thibault Damour<sup>3</sup>

<sup>1</sup>TAPIR, California Institute of Technology, Pasadena, California, USA

<sup>2</sup>DiFeST, University of Parma, I-43124 Parma, Italy

<sup>3</sup>Institut des Hautes Etudes Scientifiques, 91440 Bures-sur-Yvette, France and

<sup>4</sup>Theoretical Physics Institute, University of Jena, 07743 Jena, Germany

(Dated: May 14, 2015)

The data analysis of the gravitational wave signals emitted by coalescing neutron star binaries requires the availability of an accurate analytical representation of the dynamics and waveforms of these systems. We propose an effective-one-body (EOB) model that describes the general relativistic dynamics of neutron star binaries from the early inspiral *up to merger*. Our EOB model incorporates an enhanced attractive tidal potential motivated by recent analytical advances in the post-Newtonian and gravitational self-force description of relativistic tidal interactions. No fitting parameters are introduced for the description of tidal interaction in the late, strong-field dynamics. We compare the model energetics and the gravitational wave phasing with new high-resolution multi-orbit numerical relativity simulations of equal-mass configurations with different equations of state. We find agreement within the uncertainty of the numerical data for all configurations. Our model is the first semi-analytical model which captures the tidal amplification effects close to merger. It thereby provides the most accurate analytical representation of binary neutron star dynamics and waveforms currently available.

PACS numbers: 04.25.D-, 04.30.Db, 95.30.Sf

*Introduction.* — One of the key aims of the upcoming detections of gravitational wave (GW) signals from coalescing binary neutron stars (BNS) is to inform us on the equation of state (EOS) of matter at supranuclear densities [1–5] via the measurement of the tidal polarizability coefficients (or Love numbers) [6–10] that enter both the interaction potential and the waveform. A necessary requirement for this program is the availability of faithful waveform models that capture the strong-gravity and tidally-dominated regime of the late-inspiral of BNS *up to merger*. Such models are presently missing; the aim of this work is to close this gap so as to help developing GW astronomy.

The theoretical modeling of BNS waveforms is challenging, and requires synergy between analytical and numerical approaches to the general relativistic two body problem. Traditional post-Newtonian (PN) analytical methods reach their limits during the late BNS inspiral, and are a major limitation for GW data analysis [5, 11, 12]. In recent years numerical relativity (NR) simulations have become fairly robust [13–18], though the achievable precision is under debate and exploring the physical parameter space at the necessary accuracy (waveform length and phase errors) is certainly out of reach [14, 16, 17]. The difficulties related to PN and NR modeling carry over in the construction of hybrid PN-NR templates [3]. Presently, the effective-one-body (EOB) formalism [19–22] offers the most accurate analytical description of the relativistic two body problem. By combining information coming both from analytical results and numerical simulations, the EOB framework succeeds in describing the energetics and the GW signals of coalescing and merging black hole binaries (BBH) [23–

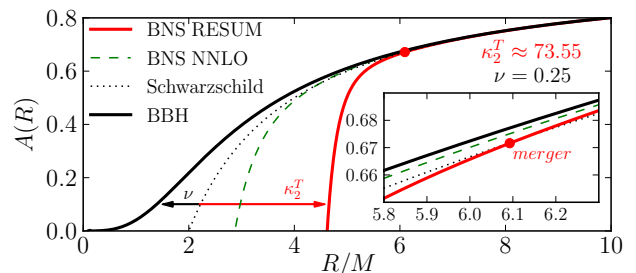


FIG. 1: The main radial gravitational potential  $A(R)$  in various EOB models. Finite-mass ratio effects ( $\nu$ ) make the gravitational interaction less attractive than the Schwarzschild relativistic potential  $A_{\text{Schw}} = 1 - 2M/R$ , while tides ( $\kappa_2^T$ , see Table I) make it more attractive (especially at short separations).

29].

The EOB model is a relativistic generalization of the well-known Newtonian property that the relative motion of a two-body system is equivalent to the motion of a particle of mass  $\mu = M_A M_B / (M_A + M_B)$  in the two-body potential  $V(R)$ . The Newtonian radial dynamics is governed by the effective potential  $V_{\text{eff}}(R; P_\varphi) = P_\varphi^2 / (2\mu R^2) + V(R)$ , where the first term, which contains the angular momentum  $P_\varphi$ , is a centrifugal potential. In the EOB formalism there is an analogous effective relativistic radial potential (setting  $G = c = 1$ ),  $W_{\text{eff}}(R; P_\varphi) = \sqrt{A(R) (\mu^2 + (P_\varphi/R)^2)}$ , where  $A(R)$  is the main radial potential. In the Newtonian approximation,  $A(R) \approx 1 + 2V(R)/\mu$ , so that  $W_{\text{eff}}(R) \approx \mu + V_{\text{eff}}(R; P_\varphi)$ . In the test-mass limit,  $A(R)$  is simply equal to the Schwarzschild potential  $A_{\text{Schw}} = 1 - 2M/R$  (where

$M \equiv M_A + M_B$ ). Beyond the test-mass limit,  $A(R)$  is a deformation of  $A_{\text{Schw}}$  by two different physical effects: (i) finite-mass ratio effects, parametrized by  $\nu \equiv \mu/M$ ; and (ii) tidal effects (in BNS systems only), parametrized by relativistic tidal polarizability parameters  $\kappa_A^{(\ell)}$  [7–10], the most important of which is the quadrupolar combination  $\kappa_2^T = \kappa_A^{(2)} + \kappa_B^{(2)}$ . Following [2, 30], tidal interactions are incorporated in the EOB formalism by a radial potential of the form  $A(R; \nu; \kappa_A^{(\ell)}) = A^0(R; \nu) + A^T(R; \kappa_A^{(\ell)})$  where  $A^0(R)$  is the EOB BBH radial potential, and  $A^T(R)$  is an additional tidal interaction piece whose structure is discussed below. Figure 1 contrasts the deformations of  $A(R; \nu; \kappa_A^{(\ell)})$  away from  $A(R; 0; 0) = A_{\text{Schw}}$  induced either by (i) finite-mass-ratio effects, which make  $A^0(R)$  less attractive, or by (ii) tidal effects, which make  $A^{\text{BNS}}(R)$  more attractive in the strong-field regime where they dominate over the repulsive finite-mass-ratio effects. Figure 1 also compares a *resummed* tidal EOB model (incorporating recent advances in the relativistic theory of tidal interactions [31–33]) with another tidal EOB model that incorporates a tidal potential treating tidal interactions in a *nonresummed way*, up to the next-to-next leading order (NNLO, fractional 2PN, see below) [34, 35]. The resummed tidal EOB model is significantly more attractive than the NNLO one at small separations. We will consider the evolution of the EOB dynamics at separations of the order of the contact between the two NSs, i.e., at the point hereafter called “merger”. The marker in the figure indicates the radial location corresponding to that merger for the resummed EOB model ( $R_{\text{mrg}} = 6.093M$ ).

The main result of this paper is to show that the resummed EOB model is significantly closer (especially near merger) to the results of new, high-resolution, multi-orbit NR simulations, than both the NNLO EOB model and the conventional T4 PN model. This breaks new ground with respect to previous EOBNR comparisons [13, 15, 16] which could never display good analytical-numerical agreement up to merger [8, 13, 15, 16], and offers the first hope of analytically modeling BNS up to merger.

*The tidal EOB models (TEOB).*— The EOB Hamiltonian is  $H_{\text{EOB}} = M\sqrt{1 + 2\nu(\hat{H}_{\text{eff}} - 1)}$  where, in the nonspinning case,  $\hat{H}_{\text{eff}}(u, p_{r_*}, p_\varphi) \equiv H_{\text{eff}}/\mu = \sqrt{A(u; \nu)(1 + p_\varphi^2 u^2 + 2\nu(4 - 3\nu)u^2 p_{r_*}^4) + p_{r_*}^2}$ , with  $u \equiv 1/r \equiv GM/(Rc^2)$ ,  $p_\varphi \equiv P_\varphi/(M\mu)$ ,  $p_{r_*} \equiv \sqrt{A/B}p_r = P_{r_*}/\mu$ , and where  $A(u; \nu) \equiv A^0(u; \nu) + A^T(u; \nu)$  and  $B(u; \nu)$  are EOB potentials. We define the BBH potential  $A^0(u; \nu)$  as the (1, 5) Padé approximant of the formal 5PN expression  $A_{5\text{PN}}^0(u; \nu) = 1 - 2u + a_3 u^3 + a_4 u^4 + (a_5^\xi(\nu) + a_5^{\text{ln}} \ln u)u^5 + (a_6^\xi(\nu) + a_6^{\text{ln}} \ln u)u^6$ . The coefficients up to 4PN, i.e. ( $a_3, a_4, a_5^\xi(\nu), a_5^{\text{ln}}$ ), are analytically known [36]. At 5PN, both  $a_6^{\text{ln}}$  and the linear-in- $\nu$  part of  $a_6^\xi(\nu)$  [50] are analytically known [31, 37]. We do not use

here the analytical knowledge of  $a_6^\xi(\nu)$ . We used instead the “effective” value  $a_6^\xi(\nu) = 3097.3\nu^2 - 1330.6\nu + 81.38$  deduced from a recent comparison between the EOB model and a sample of NR data [38, 39]. The tidal contribution to  $A(r)$  (omitting the negligible gravitomagnetic part [8]) is

$$A_T^{(+)}(u; \nu) \equiv - \sum_{\ell=2}^4 \left[ \kappa_A^{(\ell)} u^{2\ell+2} \hat{A}_A^{(\ell+)} + (A \leftrightarrow B) \right], \quad (1)$$

where  $\kappa_A^{(\ell)} = 2k_A^\ell (X_A/C_A)^{2\ell+1} M_B/M_A$ ,  $X_{A,B} \equiv M_{A,B}/M$ ,  $k_{A,B}^{(\ell)}$  are the dimensionless Love numbers [7–10] and  $C_{A,B} \equiv (M/R_*)_{A,B}$  the stars compactnesses with  $R_{*A,B}$  the areal radii. In the equal-mass case, the EOS information is essentially encoded in the total dimensionless *quadrupolar* tidal coupling constant  $\kappa_2^T \equiv \kappa_A^{(2)} + \kappa_B^{(2)}$ . The relativistic correction factors  $\hat{A}_A^{(\ell+)}$  formally include all the high PN corrections to the leading-order. The choice of  $\hat{A}_A^{(\ell+)}$  defines the two tidal EOB models of this paper. The NNLO tidal EOB model,  $\text{TEOB}_{\text{NNLO}}$ , is defined by using the PN-expanded, fractionally 2PN accurate, expression  $\hat{A}_A^{(\ell+)\text{NNLO}} = 1 + \alpha_1^{(\ell)} u + \alpha_2^{(\ell)} u^2$  with  $\alpha_{1,2}^{(2),(3)} \neq 0$  and  $\alpha_{1,2}^{(4)} = 0$  [35]. The resummed tidal EOB model,  $\text{TEOB}_{\text{Resum}}$ , is defined by using for the  $\ell = 2$  term in Eq. (1) the expression

$$\hat{A}_A^{(2+)}(u) = 1 + \frac{3u^2}{1 - r_{\text{LR}}u} + \frac{X_A \tilde{A}_1^{(2+)\text{1SF}}}{(1 - r_{\text{LR}}u)^{7/2}} + \frac{X_A^2 \tilde{A}_2^{(2+)\text{2SF}}}{(1 - r_{\text{LR}}u)^p}, \quad (2)$$

where the functions  $\tilde{A}_1^{(2+)\text{1SF}}(u)$  and  $\tilde{A}_2^{(2+)\text{2SF}}(u)$  are defined as in [33], and where we choose  $p = 4$  for the exponent. The  $\ell = 3, 4$  contributions of the resummed model are taken as in the NNLO model. A key prescription here is to use as pole location in Eq. (2) the light ring  $r_{\text{LR}}(\nu; \kappa_A^{(\ell)})$  (i.e., the location of the maximum of  $A^{\text{NNLO}}(r; \nu; \kappa_A^{(\ell)})/r^2$ ) of the NNLO tidal EOB model [35]. The radial part of radiation reaction,  $\mathcal{F}_r = 0$ , is always set to zero [29, 38]; the tidal part of radiation reaction is completed with the next-to-leading-order tidal contribution [2, 30, 34].

*NR simulations.*— Simulations are performed with the BAM code [40, 41], which solves the Z4c formulation of Einstein’s equations [42, 43] and general relativistic hydrodynamics. The setup used here is similar to that of [15, 44], numerical details will be discussed elsewhere. We consider equal-mass binaries in which the fluid is described either by a  $\Gamma = 2$  polytropic EOS enforcing isentropic evolutions [14, 15], or by a piecewise polytropic representation of cold EOS [45] adding a  $\Gamma_{\text{th}} = 1.75$  thermal pressure component [16]. All configurations (Table I) are simulated at multiple resolutions. The simulations of (SLy,  $\Gamma_2151$ , H4) use three resolutions with ( $64^3, 96^3, 128^3$ ) grid points resolving the star diameter, while for (2B,  $\Gamma_2164$ , MS1b) only the ( $64^3, 96^3$ )

TABLE I: BNS configurations and phasing results. From left to right: name, EOS,  $\kappa_2^T$ , TEOB<sub>NNLO</sub> light-ring location, star compactnesses  $\mathcal{C}_{A,B}$  and gravitational masses in isolation, initial Arnowitt-Deser-Misner (ADM) mass and angular momentum, ( $M_{\text{ADM}}^0, \mathcal{J}_{\text{ADM}}^0$ ). The phase differences  $\Delta\phi^X \equiv \phi^X - \phi^{\text{NR}}$ , where  $X = \text{TT4, TEOB}_{\text{NNLO, TEOB}_{\text{Resum}}$  labels various analytical models, are reported at the moment of NR merger ( $0.11 \lesssim M\omega_{22}^{\text{mrg}} \lesssim 0.19$ ) as well as the corresponding NR uncertainty  $\delta\phi_{\text{NRmrg}}^{\text{NR}}$ . The resummed TEOB<sub>Resum</sub> model displays the best agreement with NR data. The phase differences, in radians, are obtained by aligning all waveforms on the frequency interval  $L_\omega \approx (0.04, 0.06)$ .

Name	EOS	$\kappa_2^T$	$r_{\text{LR}}$	$\mathcal{C}_{A,B}$	$M_{A,B}[M_\odot]$	$M_{\text{ADM}}^0[M_\odot]$	$\mathcal{J}_{\text{ADM}}^0[M_\odot^2]$	$\Delta\phi_{\text{NRmrg}}^{\text{TT4}}$	$\Delta\phi_{\text{NRmrg}}^{\text{TEOB}_{\text{NNLO}}}$	$\Delta\phi_{\text{NRmrg}}^{\text{TEOB}_{\text{Resum}}}$	$\delta\phi_{\text{NRmrg}}^{\text{NR}}$
2B135	2B	23.9121	3.253	0.2049	1.34997	2.67762	7.66256	-1.25	-0.19	+0.57 <sup>a</sup>	$\pm 4.20$
SLy135	SLy	73.5450	3.701	0.17381	1.35000	2.67760	7.65780	-2.75	-1.79	-0.75	$\pm 0.40$
$\Gamma_2164$	$\Gamma = 2$	75.0671	3.728	0.15999	1.64388	3.25902	11.11313	-2.29	-1.36	-0.31	$\pm 0.90$
$\Gamma_2151$	$\Gamma = 2$	183.3911	4.160	0.13999	1.51484	3.00497	9.71561	-2.60	-1.92	-1.27	$\pm 1.20$
H4135	H4	210.5866	4.211	0.14710	1.35003	2.67768	7.66315	-3.02	-2.43	-1.88	$\pm 1.04$
MS1b135	MS1b	289.8034	4.381	0.14218	1.35001	2.67769	7.66517	-3.25	-2.84	-2.45	$\pm 3.01$

<sup>a</sup> This value is the dephasing at the moment of TEOB<sub>Resum</sub> merger, which occurs  $\approx 30M$  before NR merger after alignment.

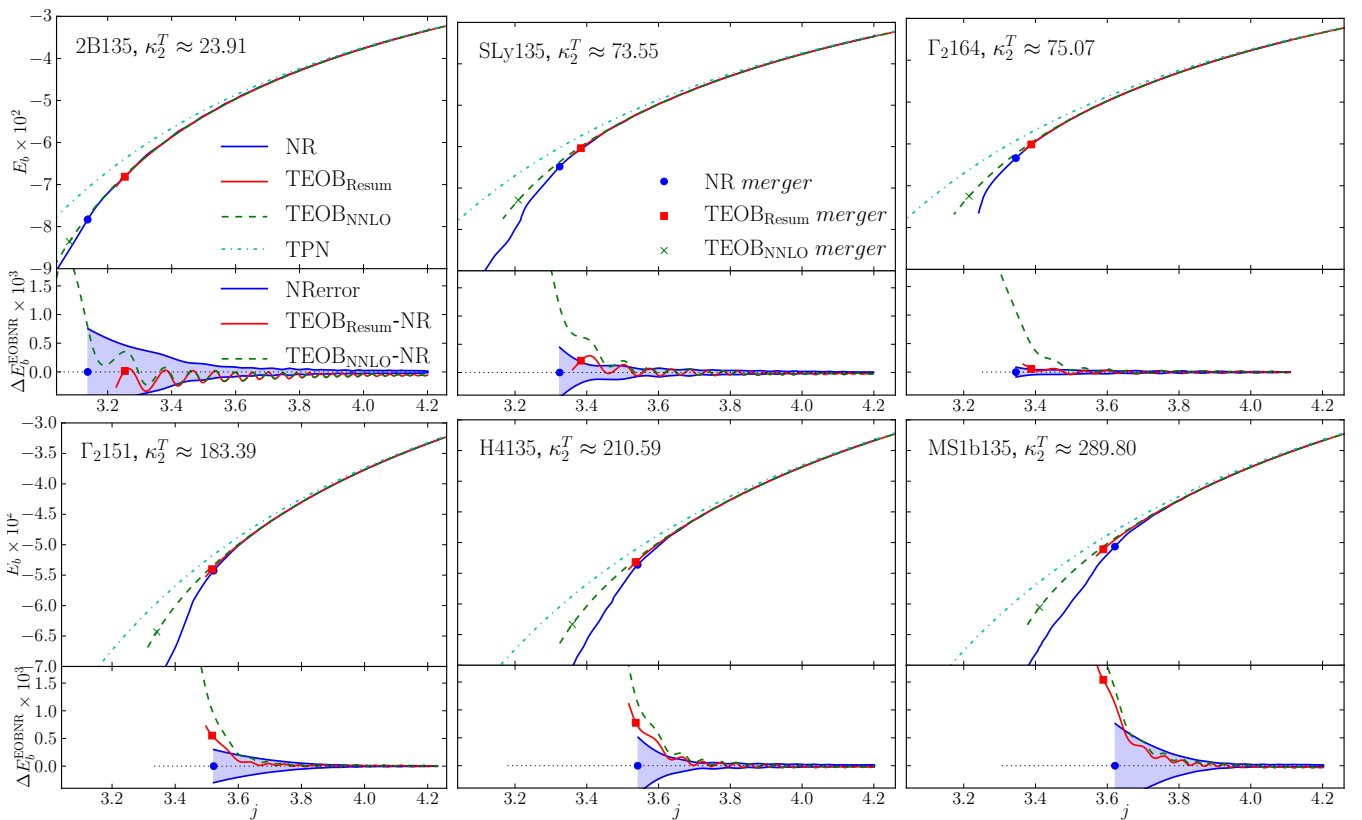


FIG. 2: Energetics: comparison between NR data, TEOB<sub>Resum</sub>, TEOB<sub>NNLO</sub> and TPN. Each bottom panel shows the two EOB-NR differences. The filled circles locate the merger points (top) and the corresponding differences (bottom). The shaded area indicates the NR uncertainty. The TEOB<sub>Resum</sub> model displays, globally, the smallest discrepancy with NR data (notably for merger quantities), supporting the theoretical, light-ring driven, amplification of the relativistic tidal factor.

resolutions are available. Numerical uncertainties are conservatively estimated as the difference between the highest and the second highest available resolutions, in an attempt at including possible systematic errors [15]. Overall, these BNS data are among the longest and most

accurate available to date.

*EOB-NR comparison: energetics.*— We compare EOB to NR energetics using the gauge-invariant relation between the binding energy and the orbital angular momentum [15, 18, 46]. We work with corre-

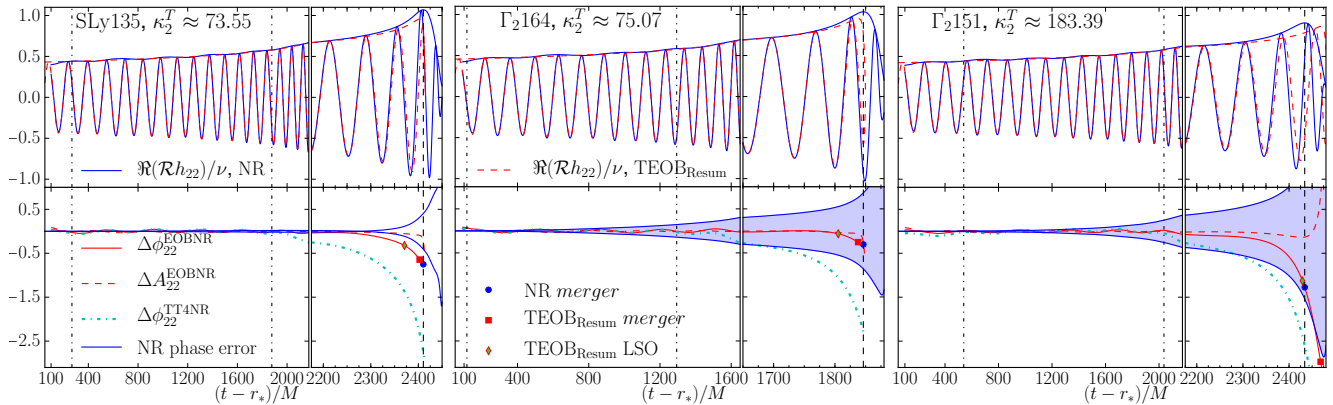


FIG. 3: Phasing and amplitude comparison (versus NR retarded time) between  $\text{TEOB}_{\text{Resum}}$ , NR and the phasing of TT4 for three representative models. Waves are aligned on a time window (vertical dot-dashed lines) corresponding to  $I_\omega \approx (0.04, 0.06)$ . The markers in the bottom panels indicate: the crossing of the  $\text{TEOB}_{\text{Resum}}$  LSO radius; NR (also with a dashed vertical line) and EOB merger moments.

sponding dimensionless quantities defined respectively as  $E_b \equiv [(M_{\text{ADM}}^0 - \Delta\mathcal{E}_{\text{rad}})/M - 1]/\nu$  and  $j \equiv (\mathcal{J}_{\text{ADM}}^0 - \Delta\mathcal{J}_{\text{rad}})/(M^2\nu)$ , where  $\Delta\mathcal{E}_{\text{rad}}$  ( $\Delta\mathcal{J}_{\text{rad}}$ ) is the radiated GW energy (angular momentum). Since the relation  $E_b(j)$  essentially captures the conservative dynamics [46], this analysis directly probes the performance of the EOB Hamiltonian, and notably the definition of  $A^T(u; \nu)$ .

The top panels of Fig. 2 compare for all EOS four energetics  $E_b(j)$ : NR,  $\text{TEOB}_{\text{Resum}}$ ,  $\text{TEOB}_{\text{NNLO}}$ , and the PN-expanded tidal energetics TPN, i.e. the (2PN accurate) expansion of the function  $E_b(j)$  in powers of  $1/c^2$ . The markers on the first three curves identify the corresponding merger points. Following [44], we define the moments of merger, intrinsically for each model, as the peak of the modulus of the corresponding  $\ell = m = 2$  waveform. The two differences  $\Delta E_b^{\text{EOBNR}}(j) = E_b^{\text{EOB}}(j) - E_b^{\text{NR}}(j)$  for  $\text{TEOB}_{\text{Resum}}$  and  $\text{TEOB}_{\text{NNLO}}$  are shown in the bottom panels. The shaded area indicates the NR uncertainty. The main findings of this comparison are: (i) TPN is always above the NR curve with a difference which becomes unacceptably large towards merger (cf. the BBH case in [46]); (ii) the location of the  $\text{TEOB}_{\text{NNLO}}$  merger point in the  $(E_b, j)$  plane is, in all cases, very significantly away from the corresponding NR merger point; (iii) by contrast, the  $\text{TEOB}_{\text{Resum}}$  merger point is, in all but one case (2B), rather close to NR, especially when  $\kappa_2^T$  is large; (iv) in all cases, the  $\text{TEOB}_{\text{Resum}}$ -NR differences (bottom panels) closely oscillate around zero during most of the simulated  $\sim$  ten orbits; (v) moreover, such differences keep staying within the NR uncertainty essentially up to (or slightly before for H4 and MS1b) the  $\text{TEOB}_{\text{Resum}}$  merger.

*EOB-NR comparison: phasing.*— The EOB resummed tidal waveform is obtained following [2, 47]. We compare the EOB and NR quadrupole waveforms  $\mathcal{R}h_{22}$ , with  $\mathcal{R}(h_+ - ih_\times) = \sum_{\ell m} \mathcal{R}h_{\ell m} - 2Y_{\ell m}$ , by us-

ing a standard (time and phase) alignment procedure in the time domain. Relative time and phase shifts are determined by minimizing the  $L^2$  distance between the EOB and NR phases integrated on a time interval corresponding to the dimensionless frequency interval  $I_\omega = M(\omega_L, \omega_R) = (0.04, 0.06)$  for all EOS, except  $\Gamma_{2164}$ , for which  $I_\omega = (0.0428, 0.06)$  as the simulation starts at higher GW frequency. Such choice for  $I_\omega$  allows one to average out the phase oscillations linked to the residual eccentricity ( $\sim 0.01$ ) of the NR simulations.

A sample of time-domain comparisons for three representative  $\kappa_2^T$ 's is shown in Fig. 3. Top panels compare the  $\text{TEOB}_{\text{Resum}}$  and NR waveforms real part and modulus. Bottom panels: (i) phase and relative amplitude differences between  $\text{TEOB}_{\text{Resum}}$  and NR; (ii) phase difference between the tidal Taylor T4 with NLO tides and 3PN waveform (TT4) and NR; and (iii) NR phase uncertainty (shaded region). The two vertical (dot-dashed) lines indicate the alignment interval; as in Fig. 2, the markers indicate the EOB (red) and NR (blue) mergers. The crossing of the radius of the  $\text{TEOB}_{\text{Resum}}$  last stable orbit (LSO) is indicated by a green marker. The time-domain comparisons shows that for all  $\kappa_2^T$  the  $\text{TEOB}_{\text{Resum}}$  model is compatible with NR data *up to merger* within NR uncertainties (at the  $2\sigma$  level or better, both in phase and amplitude). Note that the TT4 phasing performs systematically worse than  $\text{TEOB}_{\text{Resum}}$ .

Figure 3 is quantitatively completed by Table I, which compares the phase differences  $\Delta\phi^X \equiv \phi^X - \phi^{\text{NR}}$  with  $X = \text{TT4}, \text{TEOB}_{\text{NNLO}}, \text{TEOB}_{\text{Resum}}$  evaluated (after time-alignment) at the moment of NR merger. The NR uncertainty at merger  $\delta\phi_{\text{NRmerg}}^{\text{NR}}$  is also listed in the table. These numbers indicate how the disagreement with NR systematically decreases when successively considering the analytical models TT4,  $\text{TEOB}_{\text{NNLO}}$  and  $\text{TEOB}_{\text{Resum}}$ . Such hierarchy of qualities among ana-

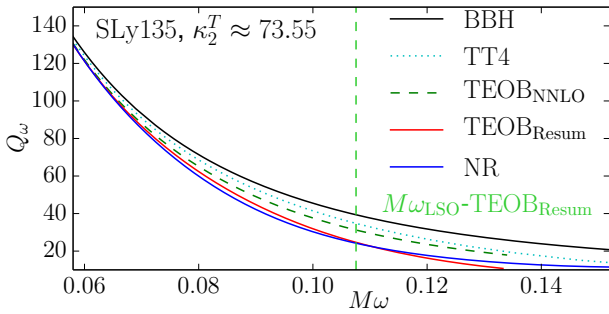


FIG. 4: Phasing comparison of various analytical models and with NR data using the gauge-invariant quantity  $Q_\omega \equiv \omega^2/\dot{\omega}$ .

lytical models is confirmed by the gauge-invariant phasing diagnostic  $Q_\omega(\omega) \equiv \omega^2/\dot{\omega}$  [13, 15]. To clean up the eccentricity-driven oscillations in the NR phase, we based our computation of  $Q_\omega^{\text{NR}}$  by starting from a simple, PN-inspired, six-parameter fit of the NR frequency as a rational function of  $x = (\nu(t_c - t)/5 + d^2)^{-1/8}$  (similarly to [48]). For each  $\kappa_2^T$  we find:  $Q_\omega^{\text{NR}} \approx Q_\omega^{\text{TEOBResum}} < Q_\omega^{\text{TEOBNNLO}} < Q_\omega^{\text{TT4}} < Q_\omega^{\text{BBH}}$  (see Fig. 4, for SLy135).

*Merger characteristics.* — The  $\text{TEOBResum}$  model, in addition to giving good energetics,  $E_b(j)$ , and phasing  $\phi(t)$  up to NR merger, has the remarkable feature of intrinsically *predicting* the frequency location and physical characteristics of merger in good quantitative agreement with NR results. This can have important consequences for building analytical GW templates. More precisely, the two quasiuniversal functional relations [44]  $E_b^{\text{mrg}}(\kappa_2^T)$  and  $M\omega^{\text{mrg}}(\kappa_2^T)$  (as well as  $j^{\text{mrg}}(\kappa_2^T)$  and the waveform amplitude at merger  $A_{22}^{\text{mrg}}(\kappa_2^T) \equiv |\mathcal{R}h_{22}^{\text{mrg}}|(\kappa_2^T)$ ) predicted by  $\text{TEOBResum}$  are close to the NR ones and significantly closer than those predicted by  $\text{TEOBNNLO}$  (while PN does not predict *any* merger characteristic). For  $E_b^{\text{mrg}}$  and  $j^{\text{mrg}}$  see Fig. 2. For  $M\omega^{\text{mrg}}(\kappa_2^T)$ , the ratio  $\omega_{\text{NR}}^{\text{mrg}}/\omega_{\text{TEOBResum}}^{\text{mrg}}$  ranges from 1.06 ( $\Gamma_2164$ ) to 1.17 (H4). For  $A_{22}^{\text{mrg}}$ , the ratio  $A_{22\text{NR}}^{\text{mrg}}/A_{22\text{TEOBResum}}^{\text{mrg}}$  ranges from 1.05 ( $\Gamma_2151$ ) to 1.15 (2B) (see also Fig. 3). Finally, after alignment, the difference  $\Delta t_{\text{mrg}} = t_{\text{mrg}}^{\text{TEOBResum}} - t_{\text{mrg}}^{\text{NR}}$  between EOB and NR merger times is only  $\sim (-30M, -8M, -9M, +34M, +51M, +92M)$  for the six models. Such agreements are remarkable as no NR-tuning of the EOB waveform was performed.

*Conclusions.* — We introduced the first tidal EOB model able to describe the energetics and waveforms of coalescing BNS from the early inspiral *up to the moment of merger*. The EOB prediction for the binary dynamics as measured by the  $E_b(j)$  curve agrees with NR data within their uncertainties for a sample of EOS spanning a significant range of tidal parameters, Fig. 2. The EOB and NR waveform phasing essentially agree within the NR uncertainties up to the moment of merger. This result is a significant improvement with respect to previ-

ous work [15, 16], notably because no parameters were tuned. Given the NR intrinsic uncertainties, and the possible residual eccentricity influence, we refrain from further calibrating the model at this stage. Once improved NR data will be available, we expect to be able to NR-inform the model, e.g. by including next-to-quasi-circular corrections to the waveform.

*Acknowledgments.* — It is a pleasure to thank D. Bini for sharing with us unpublished results about the gravitomagnetic tides, and M. Ujevic for providing us with the NR initial data. The EOB code developed here is publicly available at [eob.ihep.fr](http://eob.ihep.fr). S.B. acknowledges partial support from the National Science Foundation under grant numbers NSF AST-1333520, PHY-1404569, and AST-1205732. Ti.D. acknowledges partial support from the DFG grant SFB/Transregio 7 “Gravitational Wave Astronomy” and the Graduierten-Akademie Jena. Computations were performed on LRZ (Munich).

- 
- [1] J. S. Read, C. Markakis, M. Shibata, K. Uryu, J. D. Creighton, et al., Phys.Rev. **D79**, 124033 (2009), 0901.3258.
  - [2] T. Damour, A. Nagar, and L. Villain, Phys.Rev. **D85**, 123007 (2012), 1203.4352.
  - [3] J. S. Read, L. Baiotti, J. D. E. Creighton, J. L. Friedman, B. Giacomazzo, et al., Phys.Rev. **D88**, 044042 (2013), 1306.4065.
  - [4] W. Del Pozzo, T. G. F. Li, M. Agathos, C. V. D. Broeck, and S. Vitale, Phys. Rev. Lett. **111**, 071101 (2013), 1307.8338.
  - [5] B. D. Lackey and L. Wade, Phys.Rev. **D91**, 043002 (2015), 1410.8866.
  - [6] E. E. Flanagan and T. Hinderer, Phys.Rev. **D77**, 021502 (2008), 0709.1915.
  - [7] T. Hinderer, Astrophys.J. **677**, 1216 (2008), 0711.2420.
  - [8] T. Damour and A. Nagar, Phys. Rev. **D80**, 084035 (2009), 0906.0096.
  - [9] T. Binnington and E. Poisson, Phys. Rev. **D80**, 084018 (2009), 0906.1366.
  - [10] T. Hinderer, B. D. Lackey, R. N. Lang, and J. S. Read, Phys. Rev. **D81**, 123016 (2010), 0911.3535.
  - [11] M. Favata, Phys.Rev.Lett. **112**, 101101 (2014), 1310.8288.
  - [12] K. Yagi and N. Yunes, Phys.Rev. **D89**, 021303 (2014), 1310.8358.
  - [13] L. Baiotti, T. Damour, B. Giacomazzo, A. Nagar, and L. Rezzolla, Phys. Rev. Lett. **105**, 261101 (2010), 1009.0521.
  - [14] S. Bernuzzi, M. Thierfelder, and B. Brügmann, Phys.Rev. **D85**, 104030 (2012), 1109.3611.
  - [15] S. Bernuzzi, A. Nagar, M. Thierfelder, and B. Brügmann, Phys.Rev. **D86**, 044030 (2012), 1205.3403.
  - [16] K. Hotokezaka, K. Kyutoku, and M. Shibata, Phys.Rev. **D87**, 044001 (2013), 1301.3555.
  - [17] D. Radice, L. Rezzolla, and F. Galeazzi, Mon.Not.Roy.Astron.Soc. **437**, L46 (2014), 1306.6052.
  - [18] S. Bernuzzi, T. Dietrich, W. Tichy, and B. Brügmann, Phys.Rev. **D89**, 104021 (2014), 1311.4443.

- [19] A. Buonanno and T. Damour, Phys. Rev. **D59**, 084006 (1999), gr-qc/9811091.
- [20] A. Buonanno and T. Damour, Phys. Rev. **D62**, 064015 (2000), gr-qc/0001013.
- [21] T. Damour, P. Jaranowski, and G. Schäfer, Phys. Rev. **D62**, 084011 (2000), gr-qc/0005034.
- [22] T. Damour, Phys. Rev. **D64**, 124013 (2001), gr-qc/0103018.
- [23] T. Damour, A. Nagar, and S. Bernuzzi, Phys.Rev. **D87**, 084035 (2013), 1212.4357.
- [24] Y. Pan, A. Buonanno, A. Taracchini, L. E. Kidder, A. H. Mroue, et al., Phys.Rev. **D89**, 084006 (2014), 1307.6232.
- [25] Y. Pan, A. Buonanno, A. Taracchini, M. Boyle, L. E. Kidder, et al., Phys.Rev. **D89**, 061501 (2014), 1311.2565.
- [26] A. Taracchini, A. Buonanno, Y. Pan, T. Hinderer, M. Boyle, et al., Phys.Rev. **D89**, 061502 (2014), 1311.2544.
- [27] T. Damour, F. Guercilena, I. Hinder, S. Hopper, A. Nagar, et al. (2014), 1402.7307.
- [28] T. Damour and A. Nagar, Phys.Rev. **D90**, 024054 (2014), 1406.0401.
- [29] T. Damour and A. Nagar, Phys.Rev. **D90**, 044018 (2014), 1406.6913.
- [30] T. Damour and A. Nagar, Phys. Rev. **D81**, 084016 (2010), 0911.5041.
- [31] D. Bini and T. Damour, Phys.Rev. **D89**, 064063 (2014), 1312.2503.
- [32] S. R. Dolan, P. Nolan, A. C. Ottewill, N. Warburton, and B. Wardell (2014), 1406.4890.
- [33] D. Bini and T. Damour, Phys.Rev. **D90**, 124037 (2014), 1409.6933.
- [34] J. E. Vines and E. E. Flanagan, Phys. Rev. **D88**, 024046 (2010), 1009.4919.
- [35] D. Bini, T. Damour, and G. Faye, Phys.Rev. **D85**, 124034 (2012), 1202.3565.
- [36] D. Bini and T. Damour, Phys.Rev. **D87**, 121501 (2013), 1305.4884.
- [37] E. Barausse, A. Buonanno, and A. Le Tiec, Phys.Rev. **D85**, 064010 (2012), 1111.5610.
- [38] T. Damour, Nagar, D. Pollney, and C. Reisswig, In Preparation (2015).
- [39] A. H. Mroue, M. A. Scheel, B. Szilagyi, H. P. Pfeiffer, M. Boyle, et al., Phys.Rev.Lett. **111**, 241104 (2013), 1304.6077.
- [40] B. Brügmann, J. A. Gonzalez, M. Hannam, S. Husa, U. Sperhake, et al., Phys.Rev. **D77**, 024027 (2008), gr-qc/0610128.
- [41] M. Thierfelder, S. Bernuzzi, and B. Brügmann, Phys.Rev. **D84**, 044012 (2011), 1104.4751.
- [42] S. Bernuzzi and D. Hilditch, Phys. Rev. **D81**, 084003 (2010), 0912.2920.
- [43] D. Hilditch, S. Bernuzzi, M. Thierfelder, Z. Cao, W. Tichy, et al., Phys. Rev. **D88**, 084057 (2013), 1212.2901.
- [44] S. Bernuzzi, A. Nagar, S. Balmelli, T. Dietrich, and M. Ujevic, Phys.Rev.Lett. **112**, 201101 (2014), 1402.6244.
- [45] J. S. Read, B. D. Lackey, B. J. Owen, and J. L. Friedman, Phys. Rev. **D79**, 124032 (2009), 0812.2163.
- [46] T. Damour, A. Nagar, D. Pollney, and C. Reisswig, Phys.Rev.Lett. **108**, 131101 (2012), 1110.2938.
- [47] T. Damour, B. R. Iyer, and A. Nagar, Phys. Rev. **D79**, 064004 (2009), 0811.2069.
- [48] M. Hannam, S. Husa, F. Ohme, D. Müller, and B. Brügmann, Phys. Rev. **D82**, 124008 (2010), 1007.4789.
- [49] D. Bini and T. Damour, Phys.Rev. **D89**, 104047 (2014), 1403.2366.
- [50] The linear-in- $\nu$  corrections are actually completely known up to 8.5PN order [49]